Journal of Physics and Chemistry of Solids 168 (2022) 110810

Contents lists available at ScienceDirect

Journal of Physics and Chemistry of Solids

journal homepage: www.elsevier.com/locate/jpcs

# Glucose electrooxidation modelling studies on carbon nanotube supported Pd catalyst with response surface methodology and density functional theory

Sefika Kaya [a,*], Berdan Ulas [b,**], Derya Duzenli [d,***], Isik Onal [e], Omer Faruk Er [c], Yonca Yilmaz [c], Ilker Tezsevin [f], Hilal Kivrak [a,g]

[a] Eskisehir Osmangazi University, Faculty of Engineering and Architectural Science, Department of Chemical Engineering, Eskişehir, 26040, Turkey
[b] Van Yuzuncu Yil University, Faculty of Engineering, Department of Mining Engineering, Van, 65000, Turkey
[c] Van Yuzuncu Yil University, Faculty of Engineering, Department of Chemical Engineering, Van, 65000, Turkey
[d] General Directorate of Mineral Research and Exploration, Ankara, 06800, Turkey
[e] Middle East Technical University, Faculty of Engineering, Department of Chemical Engineering, Ankara, 06800, Turkey
[f] Department of Applied Physics, Eindhoven University of Technology, P.O. Box 513, 5600 MB Eindhoven, The Netherlands
[g] Translational Medicine Research and Clinical Center, Eskisehir Osmangazi University, 26040, Eskisehir, Turkey

ARTICLE INFO

*Keywords:*
Palladium
Carbon nanotube
Glucose electrooxidation
Response surface methodology
Density functional theory

ABSTRACT

In this study, carbon nanotube supported Pd catalysts (Pd/CNT) are synthesized at different weight percentages by the sodium borohydride ($NaBH_4$) reduction method to investigate catalytic performance of glucose electrooxidation reaction. 0.5% Pd/CNT, 3% Pd/CNT, and 7% Pd/CNT catalysts are characterized by using X-ray diffraction (XRD), electron microscopy with energy dispersive X-ray (SEM-EDX), and $N_2$ adsorption-desorption measurements. The average particle size and surface area of 3% Pd/CNT catalyst are determined as 46.33 nm and 129.48 $m^2/g$, respectively. Characterization results indicate that Pd/CNT catalysts are successfully prepared by $NaBH_4$ reduction method. Cyclic voltammetry measurements are performed to investigate the effect of Pd loading for the glucose electrooxidation. CV results reveal that 3% Pd/CNT catalyst exhibits best glucose electrooxidation activity. Following this, experimental optimization is performed to obtain maximum glucose electrooxidation activity via response surface methodology (RSM). Estimated and experimental specific activities at optimum experimental conditions are assigned as 6.186 and 5.832 $mA/cm^2$, respectively. To understand the glucose electrooxidation activity on the surface of Pd/CNT, surface modeling is also performed with density functional theory (DFT) method to investigate adsorption of glucose molecule on CNT supported Pd surface. The DFT results emphasize that the addition of Pd atom to the CNT structure significantly improves the catalytic performance in glucose electrooxidation.

## 1. Introduction

The reduction of traditional energy sources such as fossil fuels and the environmental problems they cause have led to the search for new and clean energy sources [1]. Fuel cells are devices that convert chemical energy into electrical energy and are called electrochemical generators [2]. Fuel cells are by-product thermal energy and water. It is an environmentally friendly energy source as there is no greenhouse gas emission [3,4]. Fuel cells have also many advantages such as high electricity generation efficiency, working with various fuel sources, no moving parts, reduced noise, and ease of operation [5,6].

Glucose is an abundant, non-toxic and non-volatile organic substance in nature. With these features, direct glucose fuel cells (DGFCs), which glucose are used as fuel, come to the fore as a clean and sustainable energy source [7,8]. A glucose molecule can theoretically release 24 electrons by oxidizing to carbon dioxide and water via 2.87 MJ/mol energy density. Practically, the overall cell reaction takes place which gluconic acid is produced and 2 electrons are released as shown in below

* Corresponding author.
** Corresponding author.
*** Corresponding author.
*E-mail addresses:* sefikakaya@ogu.edu.tr, sefikakaya48@gmail.com (S. Kaya), berdanulas@yyu.edu.tr (B. Ulas), duzenlid@gmail.com (D. Duzenli).

https://doi.org/10.1016/j.jpcs.2022.110810
Received 9 March 2022; Received in revised form 19 May 2022; Accepted 20 May 2022
Available online 25 May 2022

**Table 1**
The maximum current density and peak potential values of various catalysts used for glucose electrooxidation.

| Catalyst | Current, mA/cm$^2$ | Peak Potential, V | Reference |
|---|---|---|---|
| Pd/CNT | 0.58 | – | [20] |
| In/CNT | 0.90 | – | |
| PdIn(90:10)/CNT | 0.97 | – | |
| PdRh/CNT | 1.45 | – | [21] |
| AuBi(80:20)/MWCNT | 1.13 | −0.039 | [22] |
| Au/C | 2.58 | 0.4 | [23] |
| Pd/C | 0.92 | 0.4 | |
| Cu/CNT | 1.12 | −0.06 | [24] |
| Ru/CNT | 1.86 | −0.01 | |
| Ir/CNT | 3.03 | 0.12 | |
| $Pd_{30}Au_{70}$/C | 3.00 | – | [25] |
| $Pd_{10}Co_1$/KB | 3.20 | 0.65 | [26] |
| Pd–NCs | 3.35 | −0.39 | [27] |
| PdPt/C | 2.60 | −0.25 | [11] |
| PtPdAu/C | 3.40 | −0.18 | |
| PdRh/C | 3.50 | 0.051 | [28] |
| $Pd_3Sn_2$/C | 3.64 | – | [29] |
| 3% Pd/CNT | 5.832 | 0.8 | This study |

[9,10].

$$C_6H_{12}O_6 + 1/2O_2 \rightarrow C_6H_{12}O_7\ E^0 = 1.256\ V \quad (1)$$

In DGFCs, electrooxidation kinetics of glucose is slow and the adsorption of the intermediate products formed leads to poisoning of the anode catalyst [11]. In recent years, studies on electrocatalysts to increase glucose activity are quite common. Electrocatalytic properties and glucose oxidation kinetics of metal electrocatalysts are highly dependent on the effective surface area [12,13]. The loading of metal catalysts on carbon-based materials increases the electrocatalytic activity for glucose oxidation [14–16]. As a catalyst support material, CNTs have superior properties such as large surface area, electrochemical stability, and high electrical conductivity [17,18]. CNTs can decrease the cost while improving the catalytic activity and stability of electrocatalysts [19]. Table 1 includes the maximum current density and peak potential values of various catalysts used for glucose electrooxidation in literature.

Design Expert software is frequently used by researchers for the optimization of parameters affecting chemical processes. Design Expert software offers methods such as D-optimal, Plackett Burman, Taguchi OA and Response Surface Method (RSM) for the optimization of critical parameters. Design Expert software proposes an experimental program within the desired limits of the experimental parameters and creates models representing the investigated system according to the obtained experimental results. In addition, the suitability and statistical significance of the proposed model can be tested with the variance analysis and various model parameters (PRESS, Adequate Precision, Determination Coefficient, Lack of fit value) provided by the Design Expert software. Although process optimization with Design Expert software was frequently reported on adsorption before, it has also been used for determination of optimum conditions for material synthesis in recent years. In this study, critical electrode preparation parameters for glucose electrooxidation were optimized with RSM combined with Central Composite Design (CCD).

Herein, the catalysts (Pd/CNT) at different Pd weight percentages by supported CNT were synthesized by the $NaBH_4$ reduction method. Pd/CNT catalyst was characterized with XRD, SEM-EDX, and $N_2$ adsorption-desorption. Glucose electrooxidation measurements of the Pd/CNT catalyst were optimized using the RSM method via CV analysis. RSM is a mathematical and statistical method which involves the analysis and design of response surfaces. RSM enables the determination of optimum conditions by developing a mathematical model with defined test data and outputs [30]. Adsorption of the glucose molecule over Pd-doped CNT surface was examined with DFT method. It is known that the interaction of the glucose molecule with the catalysts is sensitive to the surface structure. Therefore, the catalytic performance varies with the type, decoration and crystallographic properties of the active sites. In order to observe this behavior two types of Pd-decorated surfaces were modeled. The first surface was prepared with the introduction of a Pd adatom on one of the C–C bridge sites of a perfect zigzag-CNT (Pd-CNT-Ads) whereas the second surface was prepared by inserting a Pd atom into the defective site of a zigzag-CNT with only one missing carbon atom (Pd-CNT-Ins). After optimization of the surface structure, the interactions of the molecules available in the alkaline medium with the surface was investigated. In the literature, there is a very limited literature on the systematic optimization of electrode preparation conditions with electrocatalysts. To our knowledge, no studies have been reported on the optimization of electrode modification with Pd/CNT for glucose electrooxidation and the mechanistical investigation of the electrochemical process with DFT. It is considered that this study may be the basis for the improvement of glucose electrooxidation activity of Pd-based ternary metallic anode catalysts to be investigated in the future.

## 2. Materials and method

### 2.1. Synthesis and characterization

The Pd/CNT catalysts at different Pd weight percentages were synthesized by the $NaBH_4$ reduction method. The calculated amount of $K_2PdCl_4$ (Sigma Aldrich, 99.99%) was weighed as the precursor salt and dissolved in purified water, and the support material CNT was added to this solution. Then the solution was stirred for 2 h, the determined amount of $NaBH_4$ solution was added dropwise. After stirring for 1 more hour, the solution was filtered, washed and dried in a vacuum oven at 85 °C.

The characterization of synthesized catalyst was performed by using XRD, SEM-EDX, TEM, and $N_2$ adsorption-desorption analytical techniques. The crystallinity of the catalyst was scrutinized with XRD (Panalytical Empyrean). The elemental composition and morphology of the catalyst was investigated via SEM-EDX (Zeiss Sigma 300). Brunauer-Emmett-Teller (BET) surface area, average particle size, pore-volume, and pore size values of the catalyst were determined by using $N_2$ adsorption-desorption (Micromeritics 3Flex).

### 2.2. Electrochemical measurements

CHI 660E potentiostat device was performed for electrochemical measurements. Glassy carbon electrode was used as working electrode, Ag/AgCl electrode as reference electrode and platinum wire as counter electrode. In order to modify the working electrode, 3 mg of the synthesized catalysts were weighed and 1 mL of Nafion solution was added and dissolved for 10 min with the help of an ultrasonic water bath. The obtained catalyst sludge was dripped onto the working electrode with a diameter of 3 mm. After the electrode surface was coated with the prepared catalyst slurry, it was allowed to dry at room temperature. Then the electrochemical measurements were taken. CV measurements were carried out in the potential range −0.6-0.8 V in 1 M KOH +0.5 M Glucose solution at 50 mV/s.

### 2.3. Response surface methodology

For the preparation of the working electrode, the effect of parameters namely the volume of catalyst transferred to the electrode surface ($V_c$, A), the exposure time of the mixture consisting of Nafion and 3% Pd/CNT to ultrasonication ($t_u$, B), and the drying time of catalyst slurry ($t_d$, C) on the specific activity for glucose electrooxidation on the Pd surface were optimized with a central composite design (CCD). Parameters of $V_c$, $t_u$, and $t_d$ were coded as A, B, and C, respectively. The distribution of experimental points determined by Design Expert 7.0 and the specific

**Table 2**
Experimental design of CCD and observed responses.

| Run | $V_c$ (μL) | $t_u$ (min) | $t_d$ (min) | Specific Activity (mA/cm$^2$) |
|---|---|---|---|---|
| 1 | 10 (+1) | 60 (+1) | 40 (+1) | 6.152 |
| 2 | 10 (+1) | 1 (−1) | 1 (−1) | 2.152 |
| 3 | 0.5 (−1) | 60 (+1) | 1 (−1) | 0.379 |
| 4 | 5.25 (0) | 30.5 (0) | 20.5 (0) | 1.140 |
| 5 | 0.5 (−1) | 60 (+1) | 40 (+1) | 1.270 |
| 6 | 5.25 (0) | 60 (+1) | 20.5 (0) | 1.986 |
| 7 | 10 (+1) | 1 (−1) | 40 (+1) | 1.116 |
| 8 | 10(+1) | 30.5 (0) | 20.5 (0) | 3.407 |
| 9 | 10 (+1) | 60 (+1) | 1 (−1) | 2.565 |
| 10 | 5.25 (0) | 30.5 (0) | 20.5 (0) | 0.925 |
| 11 | 5.25 (0) | 30.5 (0) | 1 (−1) | 0.985 |
| 12 | 5.25 (0) | 30.5 (0) | 20.5 (0) | 1.206 |
| 13 | 5.25 (0) | 30.5 (0) | 20.5 (0) | 1.243 |
| 14 | 5.25 (0) | 30.5 (0) | 40 (+1) | 4.423 |
| 15 | 0.5 (−1) | 1 (−1) | 1 (−1) | 2.126 |
| 16 | 5.25 (0) | 30.5 (0) | 20.5 (0) | 1.238 |
| 17 | 5.25 (0) | 30.5 (0) | 20.5 (0) | 1.211 |
| 18 | 5.25 (0) | 1 (−1) | 20.5 (0) | 0.731 |
| 19 | 0.5 (−1) | 30.5 (0) | 20.5 (0) | 1.202 |
| 20 | 0.5 (−1) | 1 (−1) | 40 (+1) | 0.789 |

activity values at these points are shown in Table 2. As can be seen from Table 2, the low, medium, and high levels of the parameters were symbolized with −1, 0, and +1, respectively. In order to determine the errors in the response value, the measurements were repeated at 6 experimental points consisting of the midpoints of the parameters from a total of 20 sets of experimental points. The compatibility of the model with the experimental results was evaluated with the ANOVA test, the coefficient of determination ($R^2$), and the plots obtained from the Design Expert 7.0 software.

### 2.4. Density functional theory computational method

Vienna ab-initio Simulation Package (VASP) version 5.4.4 has been used for the all DFT calculations reported in this work [31,32]. The projector augmented wave (PAW) versions of the ultrasoft pseudo potentials was employed to describe electron-ion interactions [33,34]. Perdew-Wang91 (PW91) exchange-correlation functional of the generalized gradient approximation (GGA) was used [35,36]. A cutoff energy of 500 eV was used as the planewave basis for all calculations. The net force acting on the ions was taken as lower than 0.015 eV/Å for the convergence criteria of the relaxation whereas the global break condition for the electronic SC-loop was set to $10^{-6}$. Initial atomic coordinates of 8 layer, (10,0) zigzag single walled carbon nanotube model, with 80 C atoms, was generated via TubeGen 3.4 nanotube structure generator. In order to avoid the periodicity in the directions perpendicular to the nanotube walls (i.e. in x and y directions), the geometric center of the obtained nanotube was placed in the center of a 25 Å × 25 Å square. Therefore, distance between parallel nanotubes were approximately 17 Å. Monkhorst-Pack procedure was used to generate *k*-point sampling for all calculations. Various 1 × 1 × n *k*-point samplings were tested over the model system for n = 2, 3, …, 12, 13 (Fig. S1) and 1 × 1 × 5 setting, resulting in a good balance with accuracy and computational cost, was used for the all reported calculations. Optimization of the model carbon nanotube was performed via consecutive volume and ionic relaxation calculations until the energy difference for consecutive calculations was less than 0.0001 eV. The volume of the optimized model structure was kept constant for the rest of the calculations. A metal atom was introduced into the system by adsorption over surface and replacing one of the lattice C atoms of the structure. Then hydroxyl (OH) and glucose ($C_6H_6O_{12}$) adsorption energetic were studied by considering multiple binding orientations of the adsorbates. Energy of adsorption ($E_{Ads}$) was computed via Equation (2),

$$E_{Ads} = E_{CNT+Adsorbate} - (E_{CNT} + E_{Adsorbate}) \quad (2)$$

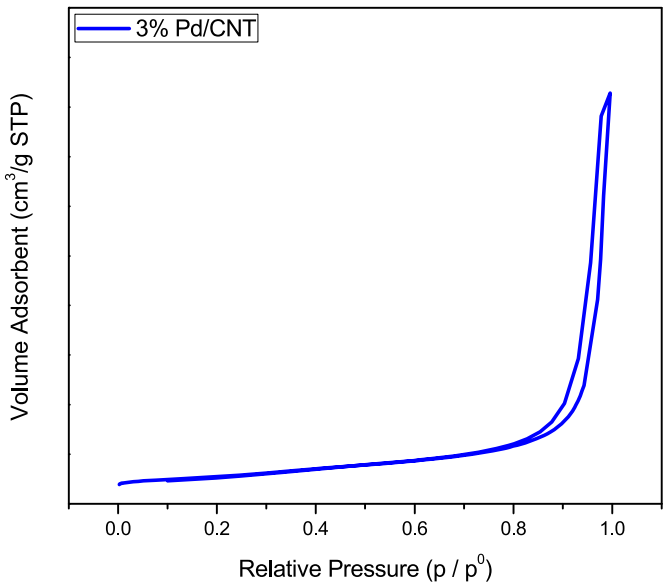


**Fig. 1.** $N_2$ adsorption-desorption isotherm of 3% Pd/CNT catalyst.

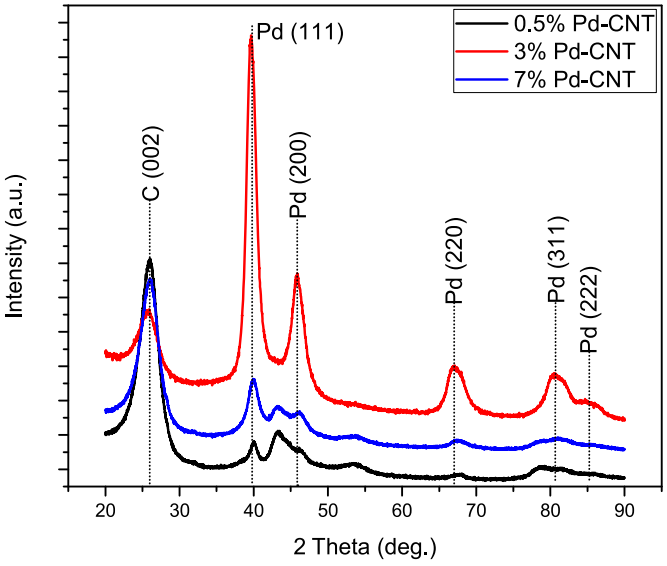


**Fig. 2.** XRD patterns of 0.5% Pd/CNT, 3% Pd/CNT, and 7% Pd/CNT catalysts.

Where $E_{CNT}$, $E_{Adsorbate}$ and $E_{CNT\ +\ Adsorbate}$ are the total energies metal doped carbon nanotube, single adsorbate molecule in gas phase, and surface (plus adsorbate) after adsorption process.

## 3. Results and discussion

### 3.1. Characterization results

0.5% Pd/CNT, 3% Pd/CNT, and 7% Pd/CNT catalysts were characterized with XRD, SEM-EDX, and $N_2$ adsorption-desorption. Result of BET measurement of 3% Pd/CNT catalyst is given in Fig. 1. It could see clearly that exhibited a V-type adsorption-desorption isotherm and H1 type hysteresis loop of 3% Pd/CNT catalyst [37,38]. Surface area from BET, average particle size, pore-volume, and pore size values were obtained as 129.48 m$^2$/g, 46.33 nm, 0.92 cm$^3$/g, and 11.71 nm, respectively.

XRD patterns of 0.5% Pd/CNT, 3% Pd/CNT, and 7% Pd/CNT catalysts are shown in Fig. 2. The C (0 0 2) plane that demonstration

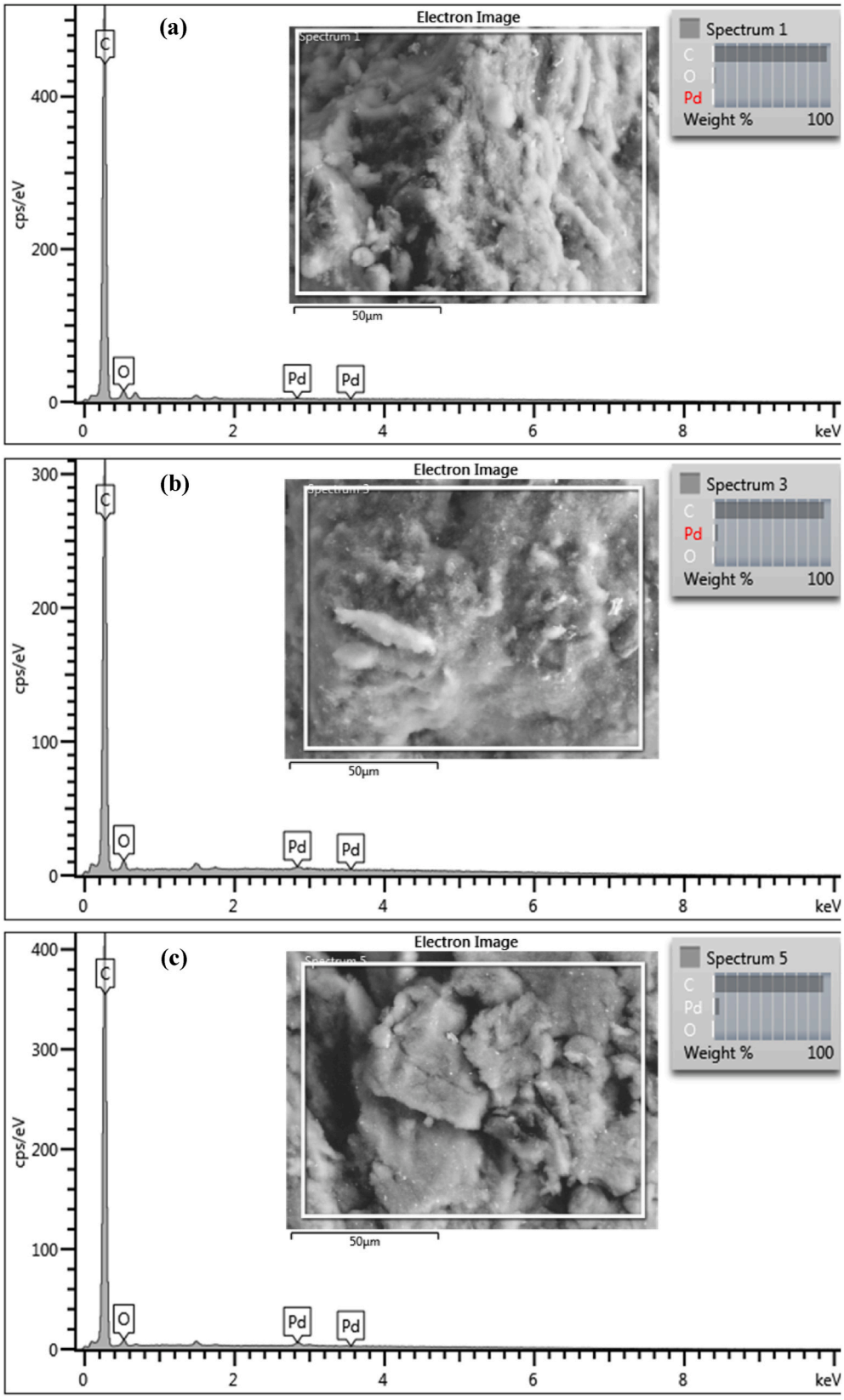


**Fig. 3.** SEM images and EDX results of a) 0.5% Pd/CNT, b) 3% Pd/CNT, and c) 7% Pd/CNT catalysts.

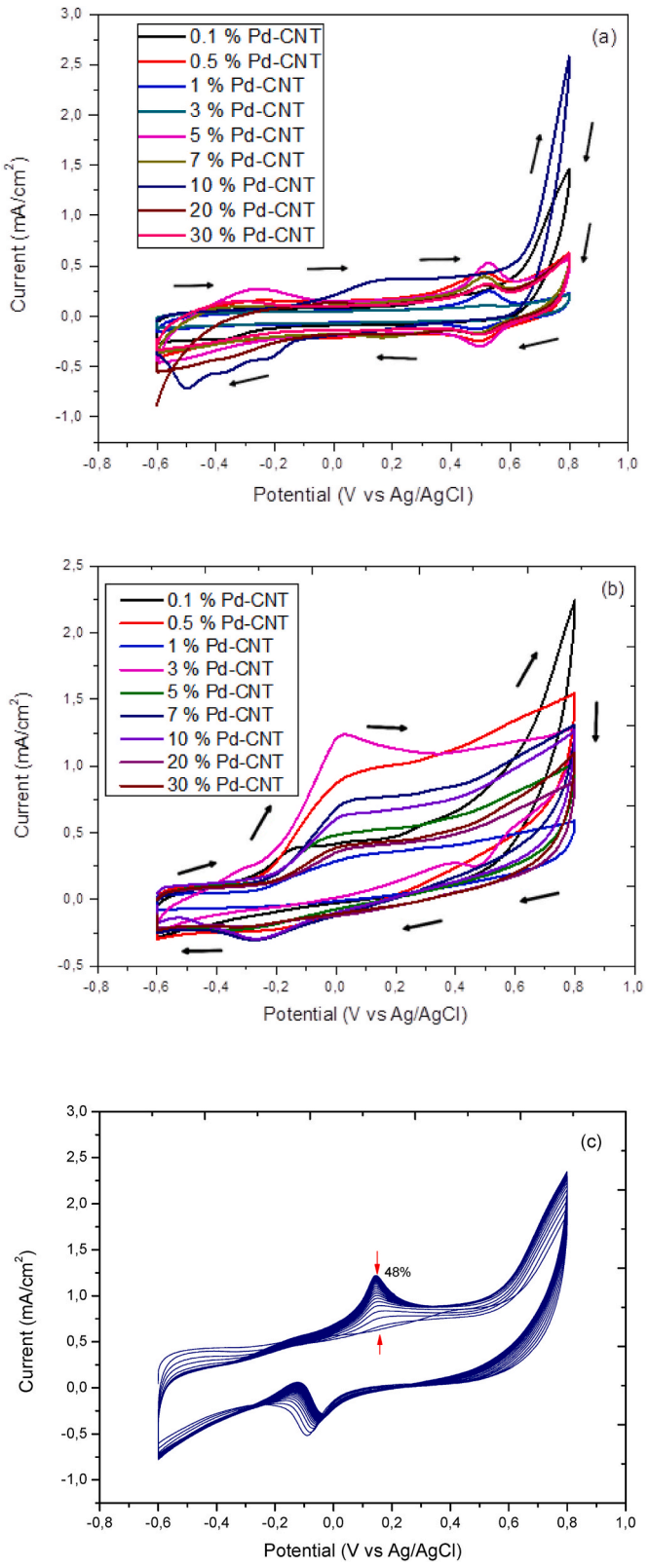


**Fig. 4.** Cyclic voltammograms on Pd/CNT catalysts prepared at varying Pd loadings in a) 1 M KOH b) 1 M KOH +0.5 M Glucose solution (50 mV/s scan rate) c) consecutive CVs on 3% Pd/CNT catalyst in 1 M KOH + 0.5 M Glucose solution.

**Table 3**
The specific activity and peak potential of Pd/CNT catalyst.

| Catalyst | Specific Activity, mA/cm$^2$ | Peak Potential, V |
|---|---|---|
| 0.1% Pd/CNT | 0.382 | −0.14 |
| 0.5% Pd/CNT | 0.956 | 0.06 |
| 1% Pd/CNT | 0.338 | 0.09 |
| 3% Pd/CNT | 1.243 | 0.02 |
| 5% Pd/CNT | 0.479 | −0.02 |
| 7% Pd/CNT | 0.739 | 0.04 |
| 10% Pd/CNT | 0.643 | 0.03 |
| 20% Pd/CNT | 0.382 | 0.05 |
| 30% Pd/CNT | 0.397 | 0.02 |

hexagonal carbon structure of CNT was obtained at 25.7$^0$ [39,40]. Furthermore, (111), (200), (220), (311), and (222) planes for all catalysts, which indicated of face-center cubic (fcc) structure of Pd nanoparticles, were found as 39.6$^0$, 45.8$^0$, 66.9$^0$, 80.6$^0$, and 85.1$^0$, respectively [41,42]. Crystallites of Pd nanoparticles over CNT for 0.5% Pd/CNT, 3% Pd/CNT, and 7% Pd/CNT catalysts via Scherrer's equation by using data of (1 1 1) planes were calculated as 8.15, 5.71, and 5.85 nm, respectively. In addition, interplanar distance of Pd nanoparticles over CNT for 0.5% Pd/CNT, 3% Pd/CNT, and 7% Pd/CNT catalysts via Bragg Law were determined using values of the Pd (1 1 1) peaks that are the most intense peaks in the XRD patterns, and this interplanar distance values were calculated as 1.62, 2.31, and 2.21 nm, respectively. Moreover, Pd (1 1 0) diffraction peaks for 0.5% Pd/CNT and 7% Pd/CNT catalysts were obtained at 43.1$^0$ [43].

SEM images and EDX results of the 0.5% Pd/CNT, 3% Pd/CNT, and 7% Pd/CNT catalysts are given in Fig. 3. Pd nanoparticles over CNT both SEM image and in the elemental map [44] could found. EDX results were clearly shown that constituted Pd nanoparticles over CNT structures. In addition, wt% values for 0.5% Pd/CNT, 3% Pd/CNT, and 7% Pd/CNT catalysts were determined as 1.21%, 3.91%, and 5.07%, respectively. These values are clearly seen that quite close 0.5%, 3%, and 7% values. It proves that XRD pattern, BET, and SEM-EDX results were prepared successfully of Pd/CNT catalyst.

### 3.2. *Electrochemical results and response surface methodology optimization*

Glucose electrooxidation activities of 0.1–30% Pd/CNT catalysts were determined by CV method at a scanning rate of 50 mV/s in the potential range of −0.6-0.8 V. These CV measurements were obtained in 1 M KOH and 1 M KOH +0.5 M Glucose solution. Fig. 4 shows the CV voltammograms in terms of specific activity on Pd/CNT catalysts. When evaluating the activity of glucose electrooxidation, the peak current in the forward scan is considered as an index. According to Fig. 4b, the peaks observed in the potential range of −0.2-0.1 V in the forward scan represent the electrooxidation due to glucose adsorption [45]. The specific activity and peak potential values of Pd/CNT catalysts are given in Table 3. The revealed results that best glucose electrooxidation activity obtained for 3% Pd/CNT catalyst with 1.243 mA/cm$^2$. As seen in Fig. 4b, the oxidation peak at 0.02 V potential was observed in the forward scan of the voltammogram of the 3% Pd/CNT catalyst, which was attributed to glucose oxidation [46–48]. Fig. 4c presents consecutive CVs (50 cycles) on 3% Pd/CNT catalyst in 1 M KOH + 0.5 M Glucose solution. The specific activity of the 3% Pd/CNT catalyst decreased as the number of CV cycles was increased. This is explained by the consumption of glucose during prolonged scanning and the poisoning of the catalyst by intermediate species produced during the glucose oxidation reaction [49]. The glucose oxidation activity on Pd/CNT catalyst decreased approximately 48% from the 1st cycle to the 50th cycle. As a similar result in the literature, Zhiani et al. reported that the glucose electrooxidation activities of Fe–Ni–Co/C and Pd/C catalysts decreased in consecutive CVs [50]. Following this, experimental optimization via response surface methodology was performed on 3% Pd/CNT catalyst.

**Table 4**
ANOVA regression model for GAEO.

| Source | Sum of Squares | df | Mean Square | F Value | p-value Prob > F |
|---|---|---|---|---|---|
| Model | 31.78 | 9 | 3.53 | 5.93 | 0.0051 significant |
| A-Vc | 9.27 | 1 | 9.27 | 15.57 | 0.0028 |
| B-tu | 2.96 | 1 | 2.96 | 4.97 | 0.0499 |
| C-td | 3.07 | 1 | 3.07 | 5.16 | 0.0464 |
| AB | 5.64 | 1 | 5.64 | 9.47 | 0.0117 |
| AC | 1.12 | 1 | 1.12 | 1.89 | 0.1997 |
| BC | 5.87 | 1 | 5.87 | 9.86 | 0.0105 |
| $A^2$ | 0.50 | 1 | 0.50 | 0.83 | 0.3824 |
| $B^2$ | 0.75 | 1 | 0.75 | 1.25 | 0.2892 |
| $C^2$ | 1.87 | 1 | 1.87 | 3.14 | 0.1069 |
| Residual | 5.95 | 10 | 0.60 | | |
| Pure Error | 0.073 | 5 | 0.015 | | |
| Cor Total | 34.74 | 10 | | | |

It was emphasized in our previous study that the effects of parameters such as $V_c$, $t_u$, and $t_d$ on glucose electrooxidation activity were statistically significant for AuBi/CNT [22]. In this study, GCE was modified with 3% Pd/CNT under the conditions indicate in Table 2. The data from Table 2 is modeled with Design Expert 7.0 software and the glucose electrooxidation on 3% Pd/CNT is well explained with a quadratic model. Accordingly, specific activity values for glucose electrooxidation on 3% Pd/CNT were given in Equation (3) and Equation (4) in terms of actual and coded values, respectively.

$$\text{Maxsimum Current Density for Glucose Electrooxidation} = +2.43822-0.26082*V_c-(7.04253*10^{-3})*t_u-0.12710*t_d+(5.99106*10^{-3})*V_ct_u+ (4.04429*10^{-3})*V_ct_d+(1.48910*10^{-3})*t_ut_d+0.018844*V_c^2-(5.98401*10^{-4})*t_u^2+ (2.16770*10^{-3})*t_d^2 \quad (3)$$

$$\text{Maxsimum Current Density for Glucose Electrooxidation} = +1.45 + 0.96*A+0.54*B+0.55*C+0.84*A*B+0.37*A*C+0.86*B*C+0.43*A^2 0.52*B^2+0.82*C^2 \quad (4)$$

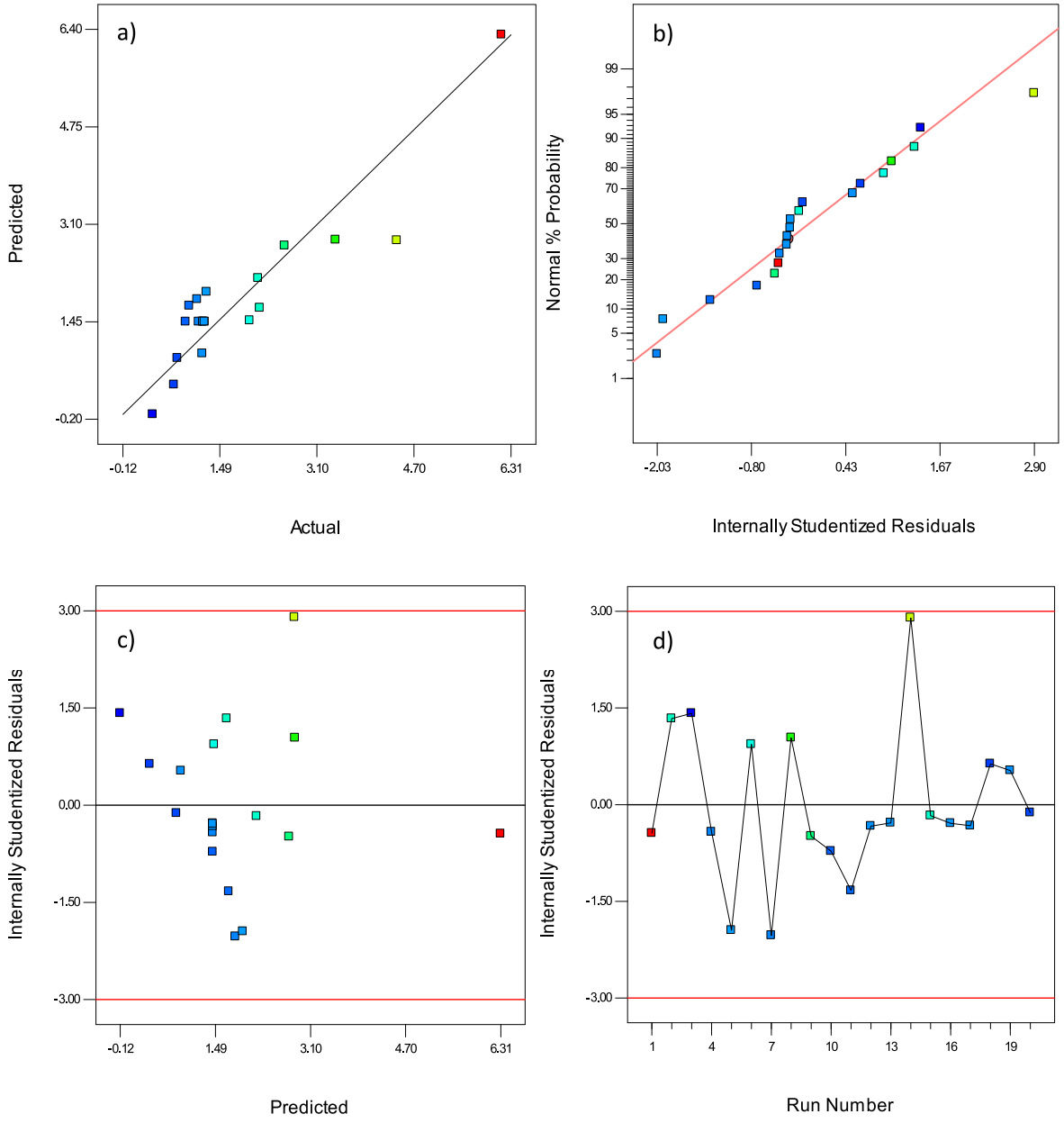


**Fig. 5.** a) Predicted versus actual b) Normal probability distribution of residuals, c) residuals versus predicted, and d) internally studentized residuals versus run for specific activity of glucose electrooxidation on 3% Pd/CNT.

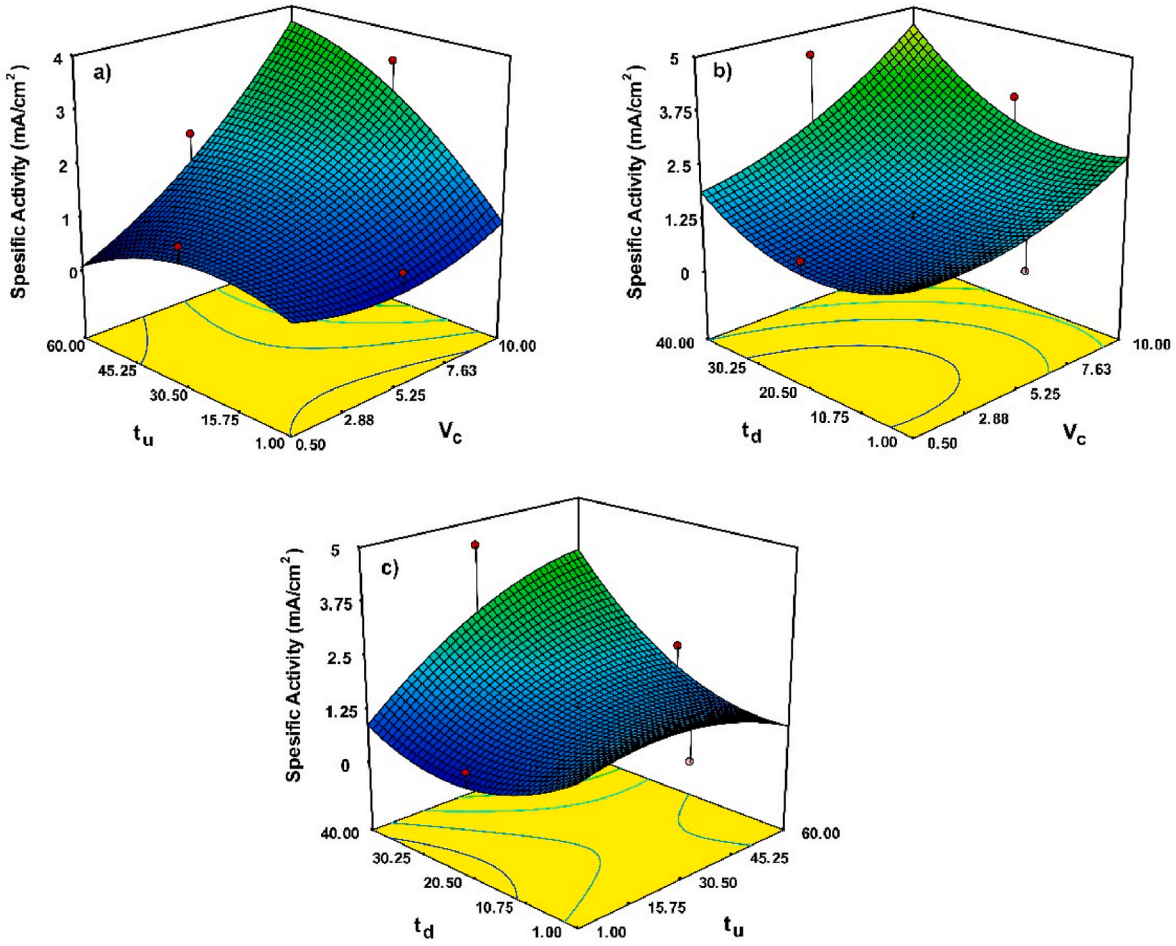


**Fig. 6.** Response surface plots of a) $t_u$ and $V_c$, b) $t_d$ and $V_c$, and c) $t_d$ and $t_u$ for glucose electrooxidation on 3% Pd/CNT.

The statistical significance of the proposed model and parameters was tested by analysis of variance (ANOVA), and the relevant results are given in Table 4. The F and Probe > F values of the proposed quadratic model for glucose electrooxidation on Pd/CNT were found to be 5.93 and 0.0051, respectively, indicating that the model is statistically significant at the 95% confidence interval. In addition, the P values of the A, B, C, AB, and BC terms of the model are less than 0.05 and are statistically significant. The regression coefficient of the proposed model was found to be 0.84, and the harmony between predicted values and the experimental data were found to be satisfactory. In addition, the standard deviation of 0.77 and the adequate precision value of 11.7 confirm the agreement between predicted and experimental data. Distribution of estimated and actual values for specific activity toward glucose electrooxidation on 3% Pd/CNT are exhibited in Fig. 5a. As can be seen from Fig. 5a, the experimental points were scattered around the diagonal despite some outliers. These results show parallelism with model parameters such as $R^2$, standard deviation, and adequate precision.

Residuals are defined as the difference between number estimated by the model and determined from the experiments, and the distribution of residuals is shown in Fig. 5b. As a result of this analysis, it is desired that the points are distributed around the straight line. Fig. 5b also show that the residuals were normally distributed along the straight line. Fig. 5c exhibit the distribution of residuals versus values predicted by the model. As can be seen from the figure, the points are randomly distributed, indicating that the variance is not constant [51]. The distribution of residuals versus test numbers was used to identify experimental and latent errors and is given in Fig. 5d. The effect of time on the response value could be revealed with this test. As could be seen from Fig. 5d, the points were scattered unevenly and without following a trend. In addition, all points were within the standard deviation range.

The response surface plots of $t_d$, $V_c$ and $t_u$ are given in Fig. 6. Fig. 6a shows the binary interaction of $t_u$ and $V_c$ for specific activity toward glucose electrooxidation on Pd/CNT. While no specific activity was observed at 1 min $t_u$, when the $t_u$ was increased to 30.5 min, the specific activity increased to 1.2018 mA/cm$^2$ ($t_d$ = 0.5 min and $V_c$ = 20.5 μL). After 30.5 min, the increase in $t_u$ caused a gradual decrease in specific activity, and the specific activity value for 60 min of $t_u$ and 0.5 μL of $V_c$ was found to be 0.01 mA/cm$^2$. Fig. 6b shows the response surface plots of $t_d$ and $V_c$ for 30.5 min of $t_u$. As the $t_d$ was increased from 1 min to 40 min, a parabolic increase was detected without observing a maximum point in specific activity, and the specific activity conditions at 40 min of $t_d$, 0.5 μL of $V_c$, and 30.5 of $t_u$ was calculated as 1.825 mA/cm$^2$ by the quadratic model. As the drying time increased, the increase in the specific activity was attributed to the stronger contact between the GCE surface and the catalyst and the lower diffusion resistance. Fig. 6c shows the 3d plots of $t_d$ and $t_u$, and it was seen that the specific activity increases with the increasing duration of drying from 1 min to 40 min, indicating that the catalyst sludge has a better adhesion to the surface and positively affects the charge transfer.

Numerical optimization was employed with using Design Expert 7.0. The optimum value of parameters namely $V_c$, $t_u$, and $t_d$ were found to be 9.93 μL, 8.83 min, and 39.84 min, respectively. The estimated and experimental specific activity under these conditions were determined as 6.186 and 5.832 mA/cm$^2$, respectively. This agreement between the calculated and experimental value from the model shows parallelism with the model tests.

**Table 5**
Formation energy and metal-surface bond length of Pd-doped CNT and the adsorption energies of species over the different surfaces.

| | Pd-CNT-Ads | Pd-CNT-Ins |
|---|---|---|
| Formation energy (eV) | −1.45 | −3.94 |
| Pd–C bond length (Å) | 2.15 | 1.98 |
| | Adsorption energy (eV) | |
| $C_6H_{12}O_6$ | −0.90 | −0.73 |
| OH | −3.15 | −3.83 |
| $C_6H_{12}O_6$ over OH-adsorbed surface | −0.66 | −0.98 |

### 3.3. Density functional theory results

Metal decorated carbon nanotubes have been studied in the literature based on many different doping procedures [52–56]. Having a doped metal as an adatom or as immersed in the surface vacancy results in different interactions between the doped metal and the substrate. Therefore, it is possible to observe with drastic catalytic activity differences for the same CNT-metal pairs with different decoration patterns. To observe this property in our study, two different metal-decorated CNTs were prepared to investigate the sensitivity of electrode surfaces to the electrolyte species.

The properties of the Pd-doped surfaces are given in Table 5. In addition to the two structures reported, Pd atom was also placed at the hollow site of the honey-ball structure; however, it migrated and made bonds with the two surface C atoms at the bridge site (Fig. 7a) as reported for Pd and Pt-decorated CNT surface [52–54]. The formation energy of Pd-CNT-Ads surface −1.45 eV and the bond length between Pd and C was 2.15 Å. An insertion of a Pd atom into the defective CNT (Pd-CNT-Ins) created more stable structure with −3.94 eV formation energy. A Pd atom protruded out of the chiral structure as shown in Fig. 7b and made three bonds with the surface C atoms at distance of 1.98 Å as reported in the literature [55,56].

After optimization of the electrode surface, the interactions of the species in the reaction medium were examined. At the alkaline medium, the electrode was surrounded by glucose and OH ions containing electrolyte. Hydroxide ion was placed at top of the Pd atom whereas the adsorption energy of glucose molecules was investigated for various initial geometries. Glucose molecule was brought closer to the both surfaces with the same orientations: O atom of OH group that bonded to the hemiacetal C atom, O atom of $CH_2OH$ group dangling out of the ring, oxygen atom of the ring and one of the OH groups of the ring.

Among various initial geometries, O atom of C–OH group dangling out of the ring made strong bond with Pd atom at a distance of 2.21 Å for Pd-CNT-Ads surface (Fig. 7c). The distance between C–O atoms of $C_6H_{12}O_6$ molecule enlarged from 1.42 Å to 1.45 Å with −0.90 eV adsorption energy. However, Pd-CNT-Ins (Fig. 7d) surface adsorbed the molecule with the same adsorption (−0.73 eV) energy regardless of the initial geometries except the last geometry (−0.43 eV). The bond length between O–Pd is 2.30 Å and C–O distance increased from 1.42 Å to 1.46 Å. The adsorption energies of OH and $C_6H_{12}O_6$ are reported in Table 5. According to these binding energy results it can be seen that OH species adsorbed more strongly over Pd atom, especially for Pd-CNT-Ins surface. Therefore, $C_6H_{12}O_6$ adsorption calculation was performed for OH-adsorbed surface to observe the effect of surface OH species as described in Incipient Hydroxyl Oxide Adatom Model (IHOAM) [57]. In the previous work we experienced that H atom of the OH group bounded to the hemiacetal carbon atom was more likely to react with the surface adsorbed OH ions. In the light of this information, only this configuration was examined for the activation of $C_6H_{12}O_6$ molecule with the

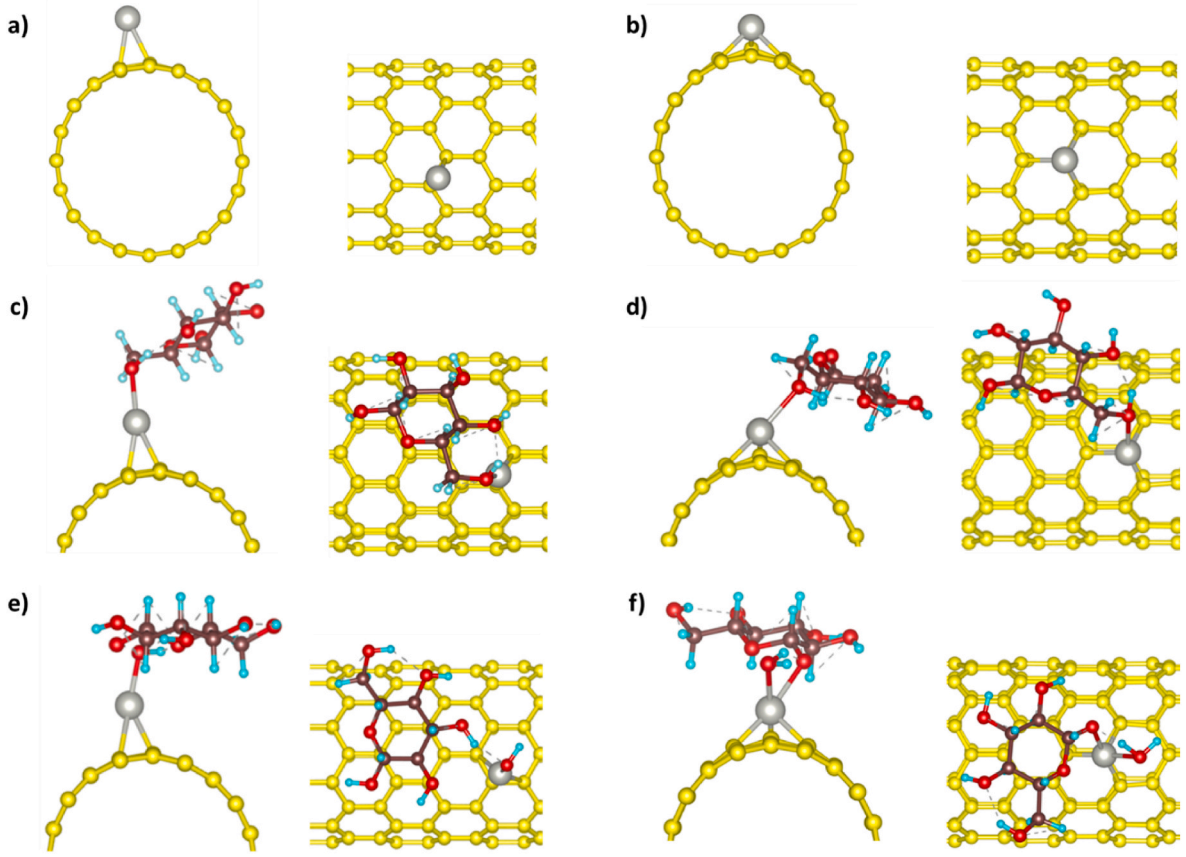


**Fig. 7.** Optimized geometries of clean (a, b), glucose adsorbed (c, d) and OH plus glucose adsorbed (e, f) Pd decorated CNT structures. The geometries on the left column represent Pd-CNT-Ads and the geometries on the right column represent Pd-CNT-Ins. (Color codes: Pd = Grey, C(CNT) = Yellow, C(Glucose) = brown, O = red, H = light blue).

surface. However, an adsorption of the OH species on Pd-CNT-Ads surface did not enhance the binding of the $C_6H_{12}O_6$ molecule and on the contrary it got weakened. The distance of O atom and nearest H atom of the $C_6H_{12}O_6$ molecule is measured as1.73 Å and the adsorption energy was calculated as −0.65 eV (Fig. 7e). On the other hand, H atom of OH group bonded to the hemiacetal carbon atom was taken from $C_6H_{12}O_6$ molecule spontaneously and formed $H_2O$ and $C_6H_{11}O_5$ molecules as expected in the model (Fig. 7f) for Pd-CNT-Ins surface. Both species anchored to the Pd atom and the length between $H_2O$ and $C_6H_{11}O_5$ and Pd atom were 2.29 Å and 2.21 Å respectively. The formation energy of the $H_2O$ molecule is −0.98 eV.

It can be inferred from these results that Pd-CNT-Ads surface structure is more suitable for development of nonenzymatic glucose sensor because of the strong affinity to the molecule. When considered in terms of the electrochemical oxidation reaction in energy applications, an insertion of the Pd atom into the CNT structure (Pd-CNT-Ins) enhanced the catalytic performance significantly in the alkaline reaction medium.

## 4. Conclusion

At present, Pd/CNT catalysts were prepared by the $NaBH_4$ reduction method at varying Pd loadings to investigate the effect of Pd loading on glucose electrooxidation activity. The characterization of the catalyst was carried out with advanced surface analysis methods such as XRD, SEM-EDX and $N_2$ adsorption-desorption. Pd fcc crystal planes were observed from the XRD pattern. SEM EDX results revealed that catalyst was prepared successfully. Cyclic voltammetry results revealed that 3% Pd/CNT catalysts exhibited the best glucose electrooxidation performance. Further experiments were performed to obtain the maximum current density while altering the optimization parameters while employing 3% Pd/CNT catalyst. The optimum experimental conditions of glucose electrooxidation were optimized by the RSM method. The optimum conditions were obtained as 9.93 μL ($V_c$), 8.83 min ($t_u$), and 39.84 min ($t_d$). Under these conditions, the estimated value (6.186 mA/cm$^2$) was determined to be very close to the experimental value (5.832 mA/cm$^2$). In roder to understand glucose adsorption mechanism on the surface, DFT method was employed. DFT calculation results revealed that the addition of Pd to the CNT surface increased glucose electrooxidation activity. Especially, the existence of OH groups on the surface cluster could enhance the glucose electrooxidation activity seriously which is in agreement with the experimental results due to the fact that glucose electrooxidation reaction occurs in the presence of OG groups coming from KOH solution.

## Credit author statement

Writing-original draft, Writing-review&editing:Sefika Kaya, Berdan Ulas, Derya Duzenli, Isik Onal, Omer Faruk Er, Yonca Yilmaz, Ilker Tezsevin, Hilal Kivrak. Conceptualization: Hilal Kivrak. Supervision: Hilal Kivrak.

## Declaration of competing interest

The authors declare that they have no known competing financial interests or personal relationships that could have appeared to influence the work reported in this paper.

## Appendix A. Supplementary data

Supplementary data to this article can be found online at https://doi.org/10.1016/j.jpcs.2022.110810.

## References


[1] M.Y.P. Peng, C.C. Chen, X.H. Peng, M. Marefati, Energy and exergy analysis of a new combined concentrating solar collector, solid oxide fuel cell, and steam turbine CCHP system, Sustain. Energy Technol. Assessments 39 (2020).

[2] K.S. Khoo, W.Y. Chia, K.X. Wang, C.K. Chang, H.Y. Leong, M.N. Bin Maaris, P. L. Show, Development of proton-exchange membrane fuel cell with ionic liquid technology, Sci. Total Environ. 793 (2021).

[3] M. Mehrpooya, B. Ghorbani, F.K. Bahnamiri, M. Marefati, Solar fuel production by developing an integrated biodiesel production process and solar thermal energy system, Appl. Therm. Eng. 167 (2020).

[4] R. Baronia, J. Goel, Baijnath, V. Kataria, S. Basu, S.K. Singhal, Electro-oxidation of ethylene glycol on Pt-Co metal synergy for direct ethylene glycol fuel cells: reduced graphene oxide imparting a notable surface of action, Int. J. Hydrogen Energy 44 (20) (2019) 10023–10032.

[5] T. Wilberforce, A. Alaswad, A. Palumbo, M. Dassisti, A.G. Olabi, Advances in stationary and portable fuel cell applications, Int. J. Hydrogen Energy 41 (37) (2016) 16509–16522.

[6] O.Z. Sharaf, M.F. Orhan, An overview of fuel cell technology: fundamentals and applications, Renew. Sustain. Energy Rev. 32 (2014) 810–853.

[7] C.H.A. Tsang, D.Y.C. Leung, Pd-Pt loaded graphene aerogel on nickel foam composite as binder-free anode for a direct glucose fuel cell unit, Solid State Sci. 71 (2017) 123–129.

[8] B.Y. Song, Y. He, Y.L. He, D. Huang, Y.W. Zhang, Experimental study on anode components optimization for direct glucose fuel cells, Energy 176 (2019) 15–22.

[9] S. Kerzenmacher, J. Ducree, R. Zengerle, F. von Stetten, Energy harvesting by implantable abiotically catalyzed glucose fuel cells, J. Power Sources 182 (1) (2008) 1–17.

[10] D. Basu, S. Basu, Synthesis, characterization and application of platinum based bi-metallic catalysts for direct glucose alkaline fuel cell, Electrochim. Acta 56 (17) (2011) 6106–6113.

[11] D. Basu, S. Basu, Performance studies of Pd-Pt and Pt-Pd-Au catalyst for electro-oxidation of glucose in direct glucose fuel cell, Int. J. Hydrogen Energy 37 (5) (2012) 4678–4684.

[12] Y. Chen, W. Schuhmann, A.W. Hassel, Electrocatalysis on gold nanostructures: is the {110} facet more active than the {111} facet? Electrochem. Commun. 11 (10) (2009) 2036–2039.

[13] K. Tao, H. Arano, P.P. Zhang, P.P. Ai, L. Han, N. Tsubaki, Enhanced hydrogen production from steam reforming of vegetable oil over bimodal ZrO2-SiO2 supported Ni catalyst, ChemistrySelect 2 (1) (2017) 527–532.

[14] C.H. Su, C.L. Sun, S.Y. Peng, J.J. Wu, Y.H. Huang, Y.C. Liao, High performance non-enzymatic graphene-based glucose fuel cell operated under moderate temperatures and a neutral solution, J. Taiwan Inst. Chem. Eng. 95 (2019) 48–54.

[15] M. Gholinejad, Z. Naghshbandi, C. Najera, Carbon-derived supports for palladium nanoparticles as catalysts for carbon-carbon bonds formation, ChemCatChem 11 (7) (2019) 1792–1823.

[16] M. Gholinejad, H. Esmailoghli, F. Khosravi, J.M. Sansano, Ionic liquid modified carbon nanotube supported palladium nanoparticles for efficient Sonogashira-Hagihara reaction, J. Organomet. Chem. 963 (2022).

[17] A. Uzundurukan, E.S. Akca, Y. Budak, Y. Devrim, Carbon nanotube-graphene supported bimetallic electrocatalyst for direct borohydride hydrogen peroxide fuel cells, Renew. Energy 172 (2021) 1351–1364.

[18] A. Brouzgou, E. Gorbova, Y. Wang, S.Y. Jing, A. Seretis, Z.X. Liang, P. Tsiakaras, Nitrogen-doped 3D hierarchical ordered mesoporous carbon supported palladium electrocatalyst for the simultaneous detection of ascorbic acid, dopamine, and glucose, Ionics 25 (12) (2019) 6061–6070.

[19] M.G. Hosseini, R. Mahmoodi, Improvement of energy conversion efficiency and power generation in direct borohydride-hydrogen peroxide fuel cell: the effect of Ni-M core-shell nanoparticles (M = Pt, Pd, Ru)/Multiwalled Carbon Nanotubes on the cell performance, J. Power Sources 370 (2017) 87–97.

[20] O.F. Er, A. Caglar, H. Kivrak, Enhanced electrochemical glucose oxidation in alkaline solution over indium decorated carbon supported palladium nanoparticles, Mater. Chem. Phys. 254 (2020).

[21] C.T. Hsieh, Y.F. Chen, P.Y. Yu, Deposition of binary Pd-Rh catalysts on nanostructured carbon supports for non-enzymatic glucose oxidation, Int. J. Hydrogen Energy 40 (43) (2015) 14857–14865.

[22] O.F. Er, B. Ulas, H. Demir Kivrak, Remarkable bismuth-gold alloy decorated on MWCNT for glucose electrooxidation: the effect of bismuth promotion and optimization via response surface methodology, Turk. J. Chem. 45 (4) (2021) 1173–+.

[23] T. Rafaideen, S. Baranton, C. Coutanceau, Highly efficient and selective electrooxidation of glucose and xylose in alkaline medium at carbon supported alloyed PdAu nanocatalysts, Appl. Catal. B Environ. 243 (2019) 641–656.

[24] O.F. Er, H. Kivrak, Highly active carbon nanotube supported iridium, copper, ruthenium catalysts for glucose electrooxidation, Energy Storage 3 (6) (2021) e271.

[25] L.L. Yan, A. Brouzgou, Y.Z. Meng, M. Xiao, P. Tsiakaras, S.Q. Song, Efficient and poison-tolerant PdxAuy/C binary electrocatalysts for glucose electrooxidation in alkaline medium, Appl. Catal. B Environ. 150 (2014) 268–274.

[26] A. Brouzgou, C. Lo Vecchio, V. Baglio, A.S. Arico, Z.X. Liang, A. Demin, P. Tsiakaras, Glucose electrooxidation reaction in presence of dopamine and uric acid over ketjenblack carbon supported PdCo electrocatalyst, J. Electroanal. Chem. 855 (2019).

[27] J.S. Ye, S.Y. Hsu, C.L. Lee, Sequential and transient electrocatalysis of glucose oxidation reactions by octahedral, rhombic dodecahedral, and cubic palladium nanocrystals, Electrochim. Acta 211 (2016) 1024–1032.

[28] A. Brouzgou, L.L. Yan, S.Q. Song, P. Tsiakaras, Glucose electrooxidation over PdxRh/C electrocatalysts in alkaline medium, Appl. Catal. B Environ. 147 (2014) 481–489.
[29] A. Brouzgou, S. Song, P. Tsiakaras, Carbon-supported PdSn and Pd3Sn2 anodes for glucose electrooxidation in alkaline media, Appl. Catal. B Environ. 158 (2014) 209–216.
[30] D. Panjiara, H. Pramanik, Optimization of process parameters using response surface methodology (RSM) for power generation via electrooxidation of glycerol in T-Shaped air breathing microfluidic fuel cell (MFC), Int. J. Hydrogen Energy 45 (58) (2020) 33968–33979.
[31] G. Kresse, J. Furthmuller, Efficiency of ab-initio total energy calculations for metals and semiconductors using a plane-wave basis set, Comput. Mater. Sci. 6 (1) (1996) 15–50.
[32] G. Kresse, J. Furthmuller, Efficient iterative schemes for ab initio total-energy calculations using a plane-wave basis set, Phys. Rev. B 54 (16) (1996) 11169–11186.
[33] G. Kresse, D. Joubert, From ultrasoft pseudopotentials to the projector augmented-wave method, Phys. Rev. B 59 (3) (1999) 1758–1775.
[34] G. Kresse, J. Hafner, NORM-CONSERVING and ultrasoft pseudopotentials for first-row and transition-elements, J. Phys. Condens. Matter 6 (40) (1994) 8245–8257.
[35] J.P. Perdew, J.A. Chevary, S.H. Vosko, K.A. Jackson, M.R. Pederson, D.J. Singh, C. Fiolhais, ATOMS, molecules, solids, and surfaces - applications OF the generalized gradient approximation for exchange and correlation, Phys. Rev. B 46 (11) (1992) 6671–6687.
[36] J.P. Perdew, Y. Wang, Accurate and simple analytic representation OF the electron-gas correlation-energy, Phys. Rev. B 45 (23) (1992) 13244–13249.
[37] K.S. Sing, R.T. Williams, Physisorption hysteresis loops and the characterization of nanoporous materials, Adsorpt. Sci. Technol. 22 (10) (2004) 773–782.
[38] Ö.F. Er, A. Cavak, A. Aldemir, H.D. Kivrak, Investigation of hydrazine electrooxidation performance of carbon nanotube supported Pd monometallic direct hydrazine fuel cell anode catalysts, MANAS Journal of Engineering 8(2) 90-98.
[39] H. Soleimani, N. Yahya, M. Baig, L. Khodapanah, M. Sabet, M. Burda, A. Oechsner, M. Awang, Synthesis of carbon nanotubes for oil-water interfacial tension reduction, Oil Gas Res 1 (1) (2015) 1000104.
[40] O.F. Er, A. Caglar, H. Kivrak, Enhanced electrochemical glucose oxidation in alkaline solution over indium decorated carbon supported palladium nanoparticles, Mater. Chem. Phys. 254 (2020) 123318.
[41] S. Navaladian, B. Viswanathan, T. Varadarajan, R. Viswanath, A rapid synthesis of oriented palladium nanoparticles by UV irradiation, Nanoscale Res. Lett. 4 (2) (2009) 181–186.
[42] O.F. Er, A. Caglar, B. Ulas, H. Kivrak, A. Kivrak, Novel carbon nanotube supported Co@ Ag@ Pd formic acid electrooxidation catalysts prepared via sodium borohydride sequential reduction method, Mater. Chem. Phys. 241 (2020) 122422.
[43] J.J. Lin, T. Mei, M.J. Lv, C.A. Zhang, Z.F. Zhao, X.B. Wang, Size-controlled PdO/graphene oxides and their reduction products with high catalytic activity, RSC Adv. 4 (56) (2014) 29563–29570.
[44] X.-Y. Liu, Y. Zhang, M.-X. Gong, Y.-W. Tang, T.-H. Lu, Y. Chen, J.-M. Lee, Facile synthesis of corallite-like Pt–Pd alloy nanostructures and their enhanced catalytic activity and stability for ethanol oxidation, J. Mater. Chem. 2 (34) (2014) 13840–13844.
[45] A. Caglar, B. Ulas, O. Sahin, H. Kivrak, Synthesis of in situ N-, S-, and B-doped few-layer graphene by chemical vapor deposition technique and their superior glucose electrooxidation activity, Int. J. Energy Res. 43 (14) (2019) 8204–8216.
[46] M. Tominaga, T. Shimazoe, M. Nagashima, I. Taniguchi, Composition-activity relationships of carbon electrode-supported bimetallic gold-silver nanoparticles in electrocatalytic oxidation of glucose, J. Electroanal. Chem. 615 (1) (2008) 51–61.
[47] S. Ben Aoun, Z. Dursun, T. Koga, G.S. Bang, T. Sotomura, I. Taniguchi, Effect of metal ad-layers on Au(111) electrodes on electrocatalytic oxidation of glucose in an alkaline solution, J. Electroanal. Chem. 567 (2) (2004) 175–183.
[48] R.R. Adzic, M.W. Hsiao, E.B. Yeager, Electrochemical oxidation OF glucose ON single-crystal gold surfaces, J. Electroanal. Chem. 260 (2) (1989) 475–485.
[49] M. Cao, H.Y. Cao, W.C. Meng, Q.X. Wang, Y. Bi, X.X. Liang, H.B. Yang, L. Zhang, M. F. Lang, J. Sun, Nickel-copper oxide nanoflowers for highly efficient glucose electrooxidation, Int. J. Hydrogen Energy 46 (56) (2021) 28527–28536.
[50] M. Zhiani, A. Abedini, S. Majidi, Comparison of electro-catalytic activity of Fe-Ni-Co/C and Pd/C nanoparticles for glucose electro-oxidation in alkaline half-cell and direct glucose fuel cell, Electrocatalysis 9 (6) (2018) 735–743.
[51] S.K. Behera, H. Meena, S. Chakraborty, B.C. Meikap, Application of response surface methodology (RSM) for optimization of leaching parameters for ash reduction from low-grade coal, Int. J. Min. Sci. Technol. 28 (4) (2018) 621–629.
[52] K.J. Li, W.C. Wang, D.P. Cao, Metal (Pd, Pt)-decorated carbon nanotubes for CO and NO sensing, Sensor. Actuator. B Chem. 159 (1) (2011) 171–177.
[53] A.J.G. Fa, V. Orazi, E.A. Gonzalez, A. Juan, I. Lopez-Corral, DFT study of beta-D-glucose adsorption on single-walled carbon nanotubes decorated with platinum. A bonding analysis, Appl. Surf. Sci. 423 (2017) 542–548.
[54] M.D. Ganji, F.S.E. Skardi, Adsorption of glucose molecule onto platinum-decorated single-walled carbon nanotubes: a dispersion-corrected DFT simulation, Fullerenes, Nanotub. Carbon Nanostruct. 23 (3) (2015) 273–282.
[55] M. Yoosefian, N. Etminan, Pd-doped single-walled carbon nanotube as a nanobiosensor for histidine amino acid, a DFT study, RSC Adv. 5 (39) (2015) 31172–31178.
[56] S. Demir, M.F. Fellah, Carbon nanotubes doped with Ni, Pd and Pt: a density functional theory study of adsorption and sensing NO, Surf. Sci. 701 (2020).
[57] G.G. Kumar, G. Amala, S.M. Gowtham, Recent advancements, key challenges and solutions in non-enzymatic electrochemical glucose sensors based on graphene platforms, RSC Adv. 7 (59) (2017) 36949–36976.